10

Elastic properties of nanocomposites with amorphous matrix

© A.A. Semenov, Y.M. Beltukov

Ioffe Institute, Russian Academy of Sciences,
St. Petersburg, Russia

E-mail: yaroslav.beltukov@mail.ioffe.ru

Received February 25, 2025
Revised April 11, 2025
Accepted April 12, 2025

This work is devoted to the theoretical study of the elastic properties of nanocomposites with an amorphous matrix, taking into account its strong local heterogeneity. The dependence of the stiffness of the nanocomposite on parameters such as the thickness of the amorphous layer, the scale of heterogeneity of the amorphous matrix, the radius of inclusions, and the distance between them is investigated. It is shown that the heterogeneity of the amorphous matrix leads to an increase in its elastic moduli near the interfaces with stiffer layers and inclusions. This results in an increase in the elastic moduli of the composite as a whole, which is determined by the ratio of the heterogeneity length scale of the amorphous matrix to the characteristic geometric size of the composite, which can be either the thickness of the amorphous layer or the radius of the nanoparticles.

Keywords: amorphous materials, nanocomposites, elasticity theory.

DOI: 10.61011/PSS.2025.04.61276.40-25

1. Introduction

Composite materials are a unique category of materials that are composed of two or more components with different physical and chemical properties. These components typically include a matrix and a reinforcing element that interact with each other to create a material with improved performance over the individual components. Composites have a wide range of applications in a variety of industries, including aviation, automotive, construction, sports, and medicine [1,2].

The high strength with low weight is the advantage of composites from the point of view of mechanical properties. This makes composites ideal for applications where light weight and strength are critical. Reinforcing elements, such as fibers or particles, ensure high tensile and flexural strength, while the matrix is typically responsible for load distribution and protection of the reinforcing components from external influences. In addition, composite materials can exhibit excellent stiffness, impact strength, and corrosion resistance characteristics.

Polymer composites obtained by adding various kinds of reinforcing particles to the polymer matrix play a major role among composite materials [3–6]. Since there are a number of polymers (polystyrene, polycarbonate, polymethylmethacrylate, etc.) that are in an amorphous state at room temperature [7–9], the study of the properties of composite materials with an amorphous matrix is an important practical task.

One of the key physical and mechanical properties of a composite material is the set of its elastic moduli (bulk modulus of elasticity, shear modulus, and etc.), which describe the linear relationship between stress and strain at small strains. It has been found that the addition of nanoparticles, even at low concentrations, can lead to a significant change in the elastic properties of the original polymer material [10–14]. For example, adding as little as 3 mass.% of SiO_2 nanoparticles to polymethyl methacrylate can increase the elastic modulus of the nanocomposite by 50 % [15].

It should be noted that not only polymers, but also various inorganic materials (amorphous SiO_2, amorphous Si, etc.) and metals can be in an amorphous state. The nature of the amorphous (glassy) state of a substance and the transition from the liquid state to the amorphous state remains one of the unsolved problems of condensed matter physics for decades [16–19]. Meanwhile, the study of nanocomposites with amorphous components (not necessarily polymer) opens up a number of new questions related to the description of the behavior of amorphous matter at scales of a few nanometers [20].

Amorphous materials exhibit spatially inhomogeneous microscopic elastic properties due to their disordered structure [21–24]. Deformation of such systems results in the formation of a complex inhomogeneous structure of atomic displacements, termed non-affine deformations in the literature. Such deformations have been observed in a wide variety of amorphous materials: metallic glasses [25], polymer hydrogels [26], supercooled liquids [27], Lennard-Jones glasses [28], and quartz glass [29]. The typical spatial scale of non-affine deformations has been estimated to be tens of particle sizes for Lennard-Jones glasses [30]. For smaller spatial scales, the classical continuum theory of elasticity cannot be applied [31].

If the size of an amorphous medium is much larger than the scale of its inhomogeneity, macroscopic elastic moduli can be used to describe the mechanical properties of this system. However, in composite systems containing amor-

phous materials, some regions may have small characteristic dimensions. An important example is nanocomposites, in which the size of the nanoinclusions can be comparable to the scale of inhomogeneity of the amorphous matrix. Therefore, it is important to study the local elastic properties of amorphous solids, especially near the interface with other materials.

It has been proposed that the elastic properties of nanocomposites can be described by the so-called three-phase model [32]. The model suggests that the structure of the polymer changes around the nanoparticle, leading to the formation of an effective interfacial region around the nanoparticle with intermediate elastic properties. The interfacial region has a strong influence on the macroscopic stiffness of the nanocomposite due to the large total surface area of the nanoparticles. At present, the three-phase model is commonly used as a phenomenological model to match the effect of inclusions on macroscopic elastic moduli obtained experimentally or by molecular dynamics [33–38].

There is direct experimental evidence showing an increase in the elastic moduli of polymeric materials near nanoparticles using atomic force microscopy [39–43]. However, such experiments are hampered by the fact that the radius of curvature of the probe can be comparable to the thickness of the interfacial region.

Molecular dynamics allows a more detailed study of the microscopic structure and properties of an amorphous material. Recent calculations have determined the spatial distribution of the local elastic moduli of the amorphous matrix and have shown their increase near different nanoparticles: epoxy resin near the boehmite nanolayer [44], polystyrene near the SiO_2 nanoparticle [45], and polyethylene oxide also near the SiO_2 nanoparticle [46]. It was shown for polystyrene that the increase in stiffness has an exponentially decreasing character with a characteristic scale of 1.4 nm, while the density of polystyrene saturates to its bulk value at much smaller distances [45].

In our previous paper [47], we proposed a theoretical method for determining the elastic properties of amorphous composite materials based on random matrix theory and derived an equation that determines the distribution of local elastic moduli. The aim of this paper is to study the elastic properties of amorphous composites in more detail. The main points of the theory used are summarized in Section 2. A thin layer of amorphous medium enclosed between two stiffer layers is considered in Section 3. An amorphous composite with rigid spherical particles is considered in Section 4. In both cases, the scale of inhomogeneity of the amorphous medium ξ can be either smaller or larger than other characteristic dimensions of the problem.

2. Elastic properties of an amorphous composite

The problem of determining the elastic properties of a composite material consisting of an amorphous matrix and nanometer-sized inclusions is nontrivial, since the classical continuum theory of elasticity is inapplicable at the scale of individual inclusions due to the strong fluctuations in the elastic properties of the amorphous matrix. It is possible to speak about a certain strain tensor $\hat{\varepsilon}(\mathbf{r})$ and stress tensor $\hat{\sigma}(\mathbf{r})$ only when averaging the corresponding characteristics over a minimal representative volume, the size of which can significantly exceed the interatomic distances and can be comparable to the size of inclusions.

In an amorphous body under load, atoms are displaced in an irregular manner at the microscopic level to minimize the elastic energy which results in non-affine deformations. The relationship between non-affine deformations and local elastic properties is also important. The number of degrees of freedom of the atoms of the amorphous material decreases near the boundary of an amorphous body with a stiffer material (inclusion or layer), which leads to suppression of non-affine deformations and an increase in the minimum possible elastic energy, i. e., an increase in the elastic moduli of the amorphous material in the boundary regions.

In order to describe this effect, it is necessary to take into account that the arrangement of atoms of an amorphous body and their displacements under the application of mechanical stress are not completely random, but obey certain rules. First of all, atoms tend to minimize elastic energy, and so the system is near a stable equilibrium position. Therefore, the matrix of force constants that describes the interaction of atoms is positively semi-definite and can be described using the Wishart ensemble within the framework of random matrix theory [48,49]. This approach allows determining the effective local elastic moduli of an amorphous material, taking into account boundary effects [47]. When speaking of effective moduli, we mean the following: a strongly fluctuating amorphous medium is replaced by a fictitious non-fluctuating medium whose response to an arbitrary mechanical action coincides with the average response of the amorphous medium to the same mechanical action. The behavior of such an effective averaged medium can be described using the classical continuum theory of elasticity.

The obtained bulk and shear elastic moduli of the amorphous body are $K(\mathbf{r}) = \alpha(\mathbf{r})K_0$ and $\mu(\mathbf{r}) = \alpha(\mathbf{r})\mu_0$, where K_0 and μ_0 are elastic moduli of the amorphous body away from its boundaries, and $\alpha(\mathbf{r})$ is the elastic contrast and obeys the differential equation [47]

$$\alpha(\mathbf{r}) = 1 + \xi^2 \Delta \ln \alpha(\mathbf{r}). \tag{1}$$

Here ξ is the scale of inhomogeneity of the amorphous body in this equation, and Δ denotes the Laplacian. The elastic contrast becomes much larger than 1 near the boundary with a stiffer body. When an amorphous medium is in contact with a non-deformable medium, the boundary condition takes the form $\alpha(\mathbf{r}) \to \infty$. Such a condition is well suited to describe polymer composites in which the elastic moduli of the inclusions significantly exceed the elastic moduli of the polymer matrix.

As shown in Ref. [47], the local elastic moduli $K(\mathbf{r})$ and $\mu(\mathbf{r})$ found can be used to describe the elastic properties even at a scale smaller than the scale of inhomogeneity because they are obtained by finding the average response of the medium to mechanical stress. Thus, knowing $K(\mathbf{r})$ and $\mu(\mathbf{r})$ we can apply the classical elasticity equations to find the response to external stress and the corresponding macroscopic elastic properties of the composite medium.

Let us consider two cases as an example. In first case, let us consider a thin layer of amorphous medium enclosed between two rigid planes at a distance w apart (Figure 1, a). Such a problem is one-dimensional and allows us to analytically investigate the stiffness of a thin layer of amorphous material. The more complicated case of a composite material with spherical inclusions of radius R will then be examined using numerical methods (Figure 1, b).

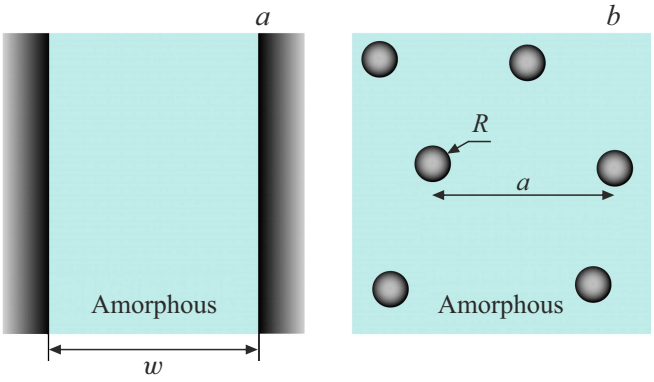

Figure 1. a — amorphous material between two infinite rigid planes at a distance w. b — an amorphous material with rigid spherical inclusions of radius R. The characteristic distance between the centers of the inclusions is a.

3. One-dimensional problem

3.1. Local elastic contrast distribution

Let us consider in more detail a one-dimensional problem in which the properties of the medium depend on only one direction. In this case, equation (1) for the local elastic contrast has the form

$$\alpha(x) = 1 + \xi^2 \frac{d^2}{dx^2} \ln \alpha(x). \tag{2}$$

For an amorphous medium enclosed between two rigid planes at a distance w apart (Figure 1, a), the coordinate x takes values from $-w/2$ (left boundary) to $w/2$ (right boundary), and the boundary conditions are of the form $\alpha(\pm w/2) = \infty$.

In the case $\xi \gg w$ the elastic contrast $\alpha(x) \gg 1$ and equation (2) has an exact solution in the form of

$$\alpha(x) = \frac{\xi^2}{w^2} \frac{4\pi^2}{1 + \cos(2\pi x/w)}. \tag{3}$$

For the more general case, the solution to equation (2) cannot be written explicitly, but it can be written in quadrature. To do this, we make the substitution

$$\alpha(x) = e^{s(t)}, \quad t = x/\xi. \tag{4}$$

Then equation (2) takes the form

$$\frac{d^2 s}{dt^2} = e^s - 1. \tag{5}$$

The solution of such an equation is expressed in quadrature:

$$t(s) = \pm \int_{s_0}^{s} \frac{1}{\sqrt{2(e^{s_1} - s_1) - E_0}} ds_1, \tag{6}$$

where $E_0 = 2(e^{s_0} - s_0)$, since the function $s(t)$ takes its minimum value s_0 at $t = 0$ due to the symmetry of the problem. Figure 2 shows the solutions (6) in the form of the dependence $s(t)$ for different values of the parameter s_0.

Each value of the parameter s_0 corresponds to a different value of the ratio w/ξ, which can be calculated based on the condition that near a rigid boundary the local elastic contrast $\alpha(x)$ tends to infinity. Therefore, the function $s(t)$ diverges at $t = \pm w/2\xi$. Extending s to infinity in equation (6), we get

$$w = 2\xi \int_{s_0}^{\infty} \frac{1}{\sqrt{2(e^{s_1} - s_1) - E_0}} ds_1. \tag{7}$$

For a fixed thickness of the amorphous layer w, the family of curves (6) for different values of the parameter s_0 describes the spatial distribution of the elastic contrast $\alpha(x)$ at different values of the inhomogeneity scale ξ (Figure 3). If the medium is homogeneous and $\xi = 0$, we obtain the trivial solution $\alpha(x) = 1$ drawn by the dashed line. If the scale of the inhomogeneity ξ is different from zero, then near the boundaries the solution has the form

$$\alpha(x - w/2) = \alpha(w/2 - x) = \frac{2\xi^2}{x^2}, \quad 0 < x \ll \xi, w, \tag{8}$$

where x is the distance to the boundary. Thus, if $\xi \ll w$, we have a region with exponential tails of elastic contrast

$$\alpha(x - w/2) = \alpha(w/2 - x) = 1 + c_1 e^{-x/\xi}, \quad \xi \ll x \ll w, \tag{9}$$

where

$$c_1 = \exp \int_0^{\infty} \left(\frac{1}{\sqrt{2(e^s - s - 1)}} - \frac{1}{e^s - 1} \right) ds \approx 2.5527. \tag{10}$$

If $\xi \gg w$, the tails merge and the solution is described by the previously derived analytic formula (3).

3.2. Macroscopic elastic moduli

An important characteristic of an amorphous layer is its stiffness, which we will feel if we move one of the

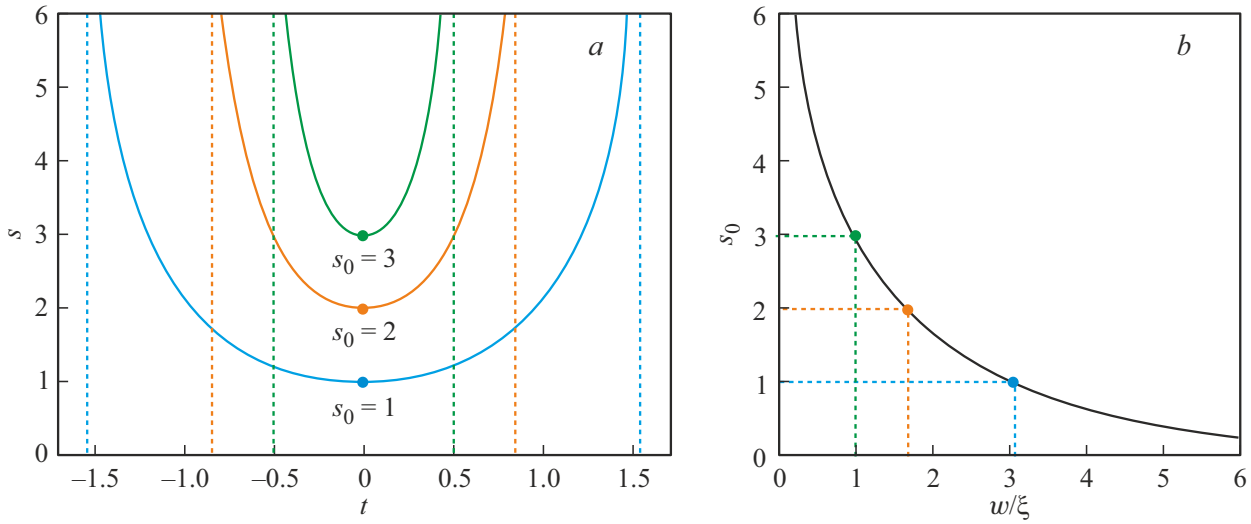

Figure 2. *a* — curves $s(t)$ for different values of the parameter s_0. The vertical dashed lines indicate the positions $\pm w/2\xi$ at which the function $s(t)$ goes to infinity. The dots indicate the position of $s_0 = s(0)$. *b* — the dependence of the parameter s_0 on the ratio of the distance between the boundaries w to the scale of the inhomogeneity ξ.

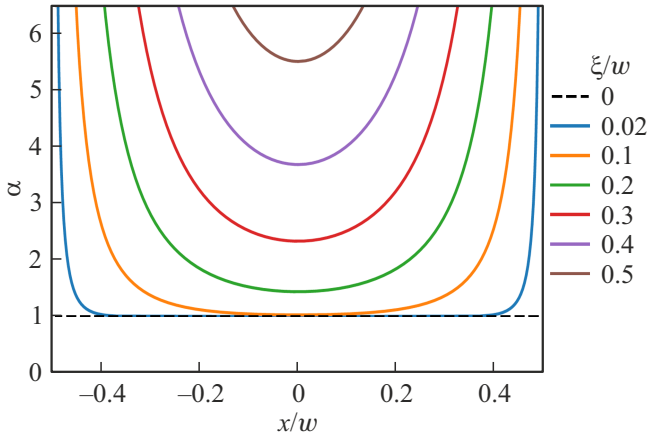

Figure 3. Distribution of local elastic contrast $\alpha(x)$ for different values of heterogeneity scale ξ. All distances are normalized by the thickness of the amorphous layer w.

boundaries relative to the other. The resulting stresses and strains can only depend on the coordinate x. The stress tensor has the form

$$\sigma_{ij}(x) = \left(K(x) - \frac{2}{3}\mu(x)\right)\delta_{ij}\varepsilon_{kk}(x) + 2\mu(x)\varepsilon_{ij}(x). \quad (11)$$

At the same time, the strain tensor $\varepsilon_{ij}(x)$ in the framework of the linear theory of elasticity has the form

$$\varepsilon_{ij}(x) = \frac{1}{2}\left(\frac{\partial u_i(x)}{\partial r_j} + \frac{\partial u_j(x)}{\partial r_i}\right), \quad (12)$$

where r_i is the coordinate x, y or z, and $u_i(x)$ is the displacement of the substance points, which depends only on the coordinate x. Hereinafter, the displacement refers to the displacement of the points of the effective medium obtained by the averaging procedure.

Substituting $K(x) = \alpha(x)K_0$ and $\mu(x) = \alpha(x)\mu_0$ into equation (11), we obtain

$$\hat{\sigma}(x) = \alpha(x) \times \begin{pmatrix} \left(K_0 + \frac{4}{3}\mu_0\right)\frac{\partial u_x(x)}{\partial x} & \mu_0\frac{\partial u_y(x)}{\partial x} & \mu_0\frac{\partial u_z(x)}{\partial x} \\ \mu_0\frac{\partial u_y(x)}{\partial x} & \left(K_0 - \frac{2}{3}\mu_0\right)\frac{\partial u_x(x)}{\partial x} & 0 \\ \mu_0\frac{\partial u_z(x)}{\partial x} & 0 & \left(K_0 - \frac{2}{3}\mu_0\right)\frac{\partial u_x(x)}{\partial x} \end{pmatrix}. \quad (13)$$

The displacement $u_i(x)$ is determined from the force balance condition

$$\frac{\partial \sigma_{ij}(x)}{\partial r_j} = 0, \quad (14)$$

integrating which we obtain a constant value of the stress tensor $\sigma_{ij}(x) = \sigma_{ij}$. Hence,

$$\frac{\partial u_i(x)}{\partial x} = \frac{A_i}{\alpha(x)}, \quad (15)$$

where

$$A_x = \frac{\sigma_{xx}}{K_0 + 4/3\mu_0}, \quad A_y = \frac{\sigma_{xy}}{\mu_0}, \quad A_z = \frac{\sigma_{xz}}{\mu_0}. \quad (16)$$

Then we can write the displacement difference of the amorphous layer boundaries as

$$u_i(w/2) - u_i(-w/2) = A_i \int_{-w/2}^{w/2} \frac{dx}{\alpha(x)}. \quad (17)$$

In describing the composite, it is convenient to pass from the spatially inhomogeneous elastic moduli $K(x)$ and

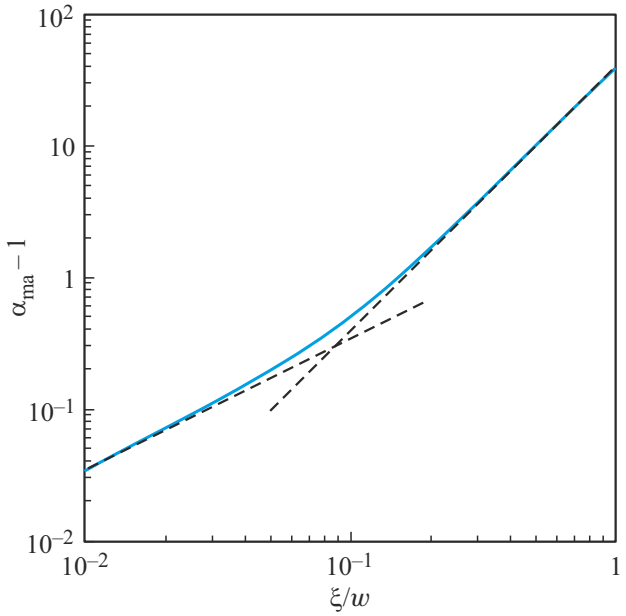

Figure 4. Dependence of the macroscopic elastic contrast of the amorphous layer α_{ma} on the ratio of the inhomogeneity scale ξ to the layer thickness w. The dashed lines show the asymptotics given by equations (20) and (21).

$\mu(x)$ to the macroscopic elastic moduli $K_{ma} = \alpha_{ma} K_0$ and $\mu_{ma} = \alpha_{ma}\mu_0$, which will give the same stiffness of the considered layer. The notion of macroscopic elastic moduli will be particularly relevant for the three-dimensional case considered next.

It should be noted that we obtain the same displacement difference $u_i(w/2) - u_i(-w/2)$ for a given stress σ_{ij} if the elastic contrast is everywhere equal to

$$\alpha_{ma} = w\left(\int\limits_{-w/2}^{w/2} \frac{dx}{\alpha(x)}\right)^{-1}. \tag{18}$$

Thus, α_{ma} is the macroscopic elastic contrast of the amorphous layer. Thus σ_{ma} denotes how many times the stiffness of the layer increases due to the influence of the boundaries, taking into account the disordered structure of the amorphous material.

The macroscopic elastic contrast α_{ma} can be expressed through quadratures as the following integral

$$\alpha_{ma} = \frac{w}{\xi}\left(\int\limits_{-w/2\xi}^{w/2\xi} e^{-s} dt\right)^{-1}$$

$$= \frac{w}{2\xi}\left(\int\limits_{s_0}^{\infty} \frac{e^{-s} ds}{\sqrt{2(e^s - s) - E_0}}\right)^{-1}, \tag{19}$$

where the relation s_0 and ξ/w is defined by formula (7). The resulting dependence of α_{ma} on ξ/w is shown in Figure 4.

When $\xi \ll w$, we have a linear growth

$$\alpha_{ma} = 1 + c_2 \frac{\xi}{w}, \tag{20}$$

where $c_2 \approx 3.47$. When $\xi \gg w$ there is an exact solution (3) for $\alpha(x)$, which gives a macroscopic elastic contrast

$$\alpha_{ma} = \frac{4\pi^2 \xi^2}{w^2}. \tag{21}$$

Thus, when the disorder is small, the macroscopic elastic contrast grows linearly with increasing ξ, and then — quadratically when the disorder becomes strong and $\xi \gg w$.

4. Three-dimensional problem

The behavior of the amorphous layer discussed in the previous section can be generalized to the case of more complex composites. For example, to the case of solid spherical inclusions in an amorphous matrix, shown in Figure 1, *b*. In this case, the local elastic contrast is determined by the three-dimensional equation (1).

If $\xi = 0$, we have a classical problem with a homogeneous medium and spherical inclusions in it. Such a problem was considered by Mori and Tanaka [50,51]. For the case of small volume fraction of rigid spherical particles, the macroscopic elastic moduli of the composite are as follows

$$K_{MT} = K_0\left(1 + 3\phi \frac{1 - \nu_0}{1 + \nu_0}\right), \tag{22}$$

$$\mu_{MT} = \mu_0\left(1 + \frac{15\phi}{2} \frac{1 - \nu_0}{4 - 5\nu_0}\right), \tag{23}$$

where $\nu_0 = (3K_0 - 2\mu_0)/(6K_0 + 2\mu_0)$ is the Poisson's ratio of the matrix, and ϕ is the volume fraction of spherical inclusions.

If the matrix is inhomogeneous, the problem becomes significantly more complicated and requires analyzing the local elastic contrast $\alpha(\mathbf{r})$ for a given scale of inhomogeneity ξ. If the distance between inclusion centers a much larger than the scale of inhomogeneity ξ and particle radius R, the local elastic contrast $\alpha(\mathbf{r})$ can be found around each inclusion independently in spherical coordinates and obtain a stepped behavior near the particle boundary

$$\alpha(r) = \frac{2R^2\xi^2}{r^2(r - R)^2}, \quad r - R \ll R, \xi \tag{24}$$

and exponential decay away from the boundary

$$\alpha(r) = 1 + c_3 \frac{R}{r} e^{-(r-R)/\xi}, \quad r - R \gg \xi, \tag{25}$$

where c_3 is a coefficient depending only on the ratio R/ξ. Thus, a shell with high values of elastic moduli is formed around each particle, whose thickness is of the order of the scale of the inhomogeneity ξ. Such a case is discussed in more detail in Ref. [47]. If $\xi \ll R, a$, the effective radius

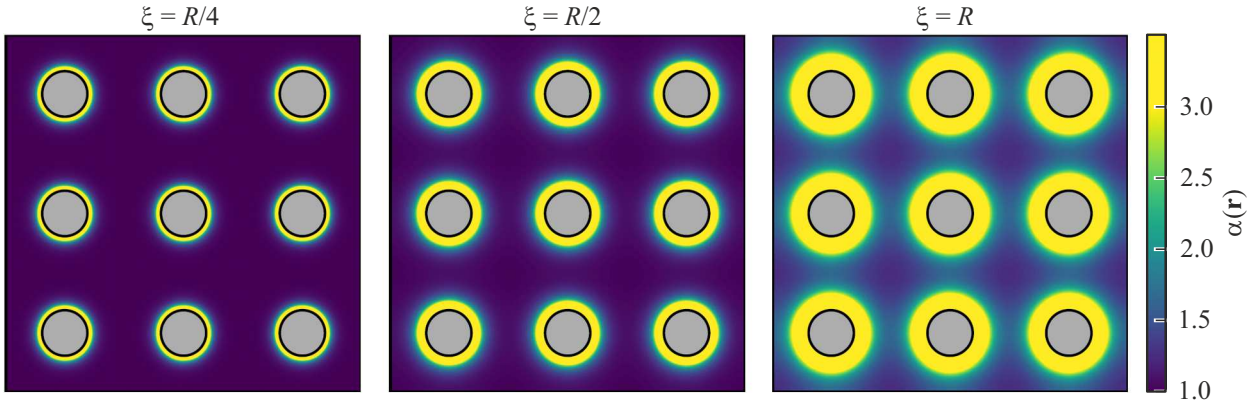

Figure 5. Distribution of elastic contrast $\alpha(\mathbf{r})$ in the plane passing through inclusion centers for composites with different values of ξ. Gray circles indicate rigid spherical inclusions with volume fraction $\phi = 3\,\%$.

of the inclusions increases by an amount of the order of ξ, giving an effective increase of ϕ and macroscopic elastic moduli proportional to ξ, which repeats the result of the one-dimensional case.

In the opposite case of extremely strong disorder, the scale of inhomogeneity is much larger than all other scales, $\xi \gg R, a$. Then $\alpha(\mathbf{r}) \gg 1$ and equation (1) becomes

$$\alpha(\mathbf{r}) = \xi^2 \Delta \ln \alpha(\mathbf{r}). \tag{26}$$

It is possible to see from this equation that for a given boundary g eometry of amorphous body $\alpha(\mathbf{r}) \sim \xi^2$. As a result, the macroscopic elastic moduli of the composite will be proportional to ξ^2, which also repeats the result of the one-dimensional case.

However, the general case where the elastic shells around the inclusions can overlap and there is an arbitrary ratio of parameters R, ξ and a is interesting. Such a problem is considerably more complicated than the one-dimensional problem discussed above. However, from general considerations, it is possible to expect that the effective elasticity of such a composite will depend on ξ/λ instead of ξ/w, where λ is some characteristic geometric dimension, which is determined by R and a. In this case, the dependence on ξ/λ will resemble the one-dimensional dependence shown in Figure 4.

Finite element methods were applied to numerically solve this problem. A composite in which spherical inclusions of radius R were located at nodes of a simple cubic lattice with period a was considered. A single cell with periodic boundary conditions was used for modeling. A second-order hexagonal mesh containing $N = 303104$ elements in this cell was used, which was described in detail in Ref. [52]. The numerical package FEniCS v0.5.2 was used for the solution [53]. The ordered arrangement of the inclusions greatly simplifies the calculation but has little effect on the elastic properties of the composite.

Figure 5 shows the results of calculating the local elastic contrast distribution in the plane passing through the centers of the spherical inclusions for different values of ξ. It can be seen that a shell with increased elastic contrast is formed around the inclusions, whose thickness depends on the scale of inhomogeneity ξ.

Figure 6 shows the calculated dependence of the increase in elastic moduli $\delta K_{\text{ma}} = K_{\text{ma}} - K_0$ and $\delta\mu_{\text{ma}} = \mu_{\text{ma}} - \mu_0$ as a function of the scale of inhomogeneity ξ with respect to the radius of nanoinclusions R at different volume fractions of nanoinclusions $\phi = 4\pi R^3/3a^3$. Results are normalized to the increment of elastic moduli in Mori-Tanaka theory $\delta K_{\text{MT}} = K_{\text{MT}} - K_0$ and $\delta\mu_{\text{MT}} = \mu_{\text{MT}} - \mu_0$. The Poisson's ratio value used in the calculation is 0.3, which corresponds to typical values for amorphous polymers.

It can be seen that for $\xi = 0$ the results are in good agreement with the classical theory and $\delta K_{\text{ma}} = \delta K_{\text{MT}}$ and $\delta\mu_{\text{ma}} = \delta\mu_{\text{MT}}$. As ξ increases, the increase in the elastic modulus around the nanoparticle begins to play a role, leading to an increase in the macroscopic elastic moduli

$$\frac{\delta K_{\text{ma}}}{\delta K_{\text{MT}}} \approx \frac{\delta\mu_{\text{ma}}}{\delta\mu_{\text{MT}}} \approx \frac{R_{\text{eff}}^3}{R^3} \tag{27}$$

due to the increased effective radius of the nanoinclusions $R_{\text{eff}} \approx R + 1.25\xi$. When $\xi \ll R$, formula (27) describes a linear increase in elastic moduli with increasing ξ. When $\xi \gg R$, the formula (27) becomes no longer applicable. But the calculation shows that elastic moduli quadratically grows in this region with the increase of ξ, as in the one-dimensional problem. Meanwhile, the most important result of the numerical calculation is that the reduced dependencies of ξ/R displayed at different ϕ are not much different from each other (Figure 6, *c* and *d*), except for the case of $R = 0.4a$ when the distance between neighboring inclusions $d = a - 2R$ becomes smaller than the radius of inclusions R. Thus, it can be concluded that the characteristic geometric size λ is determined by the particle radius R and depends weakly on the distance between the particle centers a. It should be noted that the shell size ξ can be either smaller than the distance between the nearest nanoinclusions d or larger than it. The position $\xi = d$ is marked with arrows in Figure 6. It can be seen that no

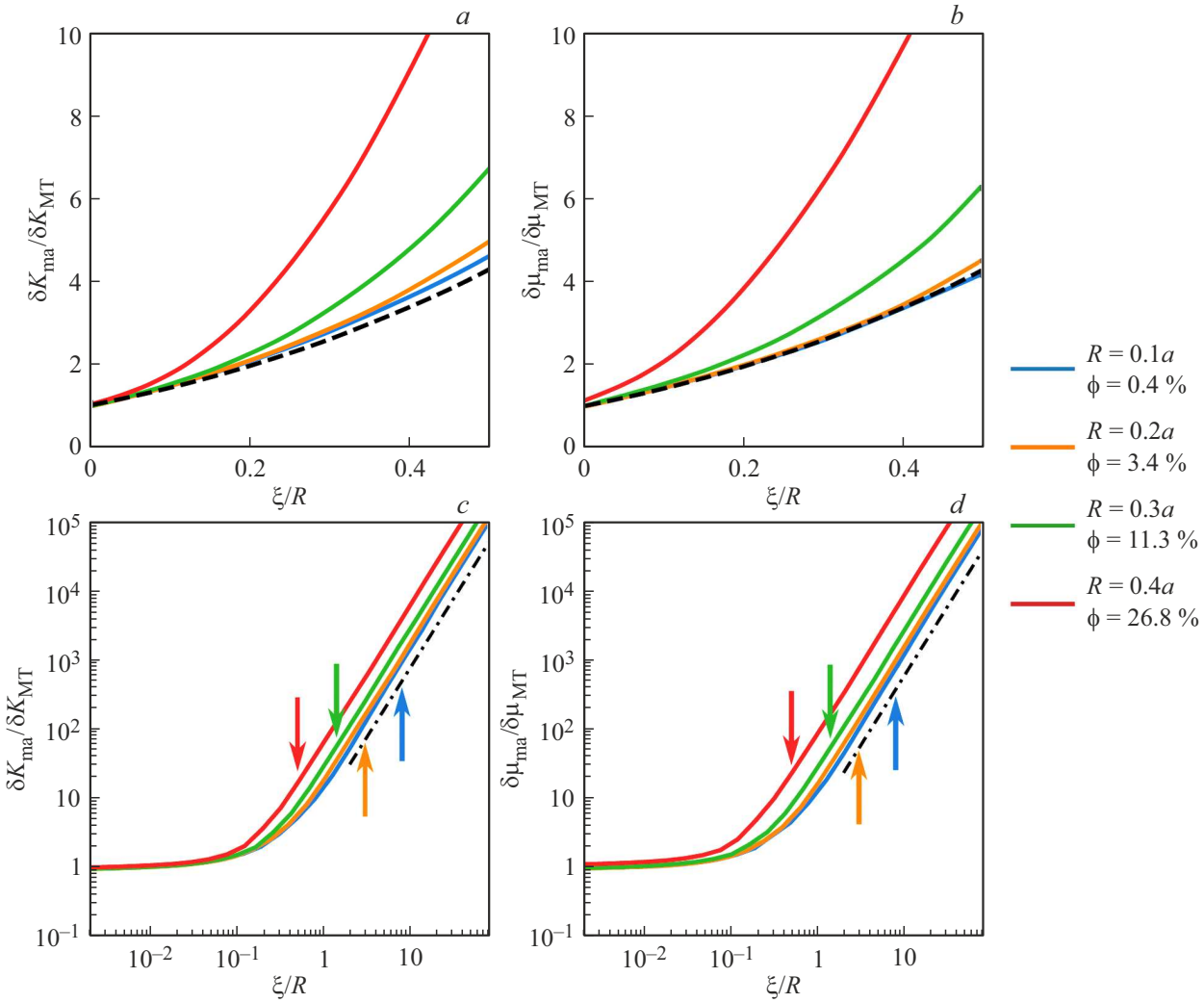

Figure 6. Dependence of the increment of macroscopic elastic moduli $\delta K_{ma} = K_{ma} - K_0$ and $\delta\mu_{ma} = \mu_{ma} - \mu_0$ as a function of the scale of inhomogeneity ξ with respect to the radius of nanoinclusions R at different volume fractions of nanoinclusions ϕ. Results normalized to the increment of elastic moduli in Mori-Tanaka theory $\delta K_{MT} = K_{MT} - K_0$ and $\delta\mu_{MT} = \mu_{MT} - \mu_0$. The Poisson's ratio is 0.3. The dashed lines in the upper panels show the dependence (27). The dashed lines in the lower panels show the asymptotics of $\delta K_{ma} \sim \xi^2/R^2$ and $\delta\mu_{ma} \sim \xi^2/R^2$. The arrows show the position d/R, where $d = a - 2R$ — the distance between the nearest nanoinclusions.

significant change in the plots at this position is observed. This is especially evident in the case of small radius of the nanoinclusions $R = 0.1a$. Thus the elastic envelopes overlap at $\xi > d$ and their effects are additive, resulting in no noticeable features when they overlap.

It is interesting to note that in the case $R \ll \xi \ll a$ the increase in elastic moduli δK_{ma} and $\delta\mu_{ma}$ is proportional to ξ^2, as in the very strong disorder limit $\xi \gg a$. This means that the effective radius of the inclusions is proportional to $\xi^{2/3}$ at $\xi \gg R$.

5. Discussion of results

The effect of inhomogeneity of the amorphous medium on the elastic properties of amorphous composites was studied in this paper. It is shown that the elastic moduli of the amorphous material increase near rigid boundaries which is associated with the suppression of non-affine deformations. This leads to an increase in the macroscopic elastic moduli of the whole composite.

The case of a layer of amorphous material enclosed between two layers of stiffer material was considered in Section 3. Such a case lends itself to analytical consideration through the application of quadrature formulas. The determination of local elastic moduli is a difficult problem for molecular dynamic modeling and even more so for experimental study. Therefore, the rigidity of the whole amorphous layer was considered, which can be determined by varying the distance between the boundaries of this layer. It is shown that the macroscopically elastic moduli thus determined increase α_{ma} times with respect to the bulk material.

It should be noted that the reasoning in this paper was based on the fact that both boundaries are rigid and well

bonded to the atoms of the amorphous material. If one of the boundaries is free, there will be no suppression of non-affine deformations near this boundary and instead of the boundary condition $\alpha(\mathbf{r}) \to \infty$ we can expect the condition $\alpha(\mathbf{r}) \approx 1$. The description of such boundaries, as well as more complex conditions with tangential slip (which occurs at the graphene or carbon nanotube boundary), requires separate consideration, which is planned in future work.

More complicated case of spherical particles in an amorphous matrix was considered in Section 4. With the help of numerical calculations it was shown that qualitatively the results fully repeat the one-dimensional case, only now a shell of thickness ξ with increased values of elastic moduli is formed around each particle, and the radius of nanoparticles R serves as the main geometric dimension. It is shown that the ratio of the scale of inhomogeneity ξ to the distance between particle centers a is not determinant. According to the obtained calculation results, when $\xi > a$, the elastic shells overlap and their effects are additive, continuing the existing trend. A noticeable deviation is observed only when the gap between particles d becomes smaller than the radius of particles R. If we have a composite in which all the particles are almost in contact, then the gap between the particles d, instead of the radius R, is likely to be the geometric dimension. In practice, however, composites with low volume fraction of inclusions are of most interest.

It should be noted that in polymeric materials nanoparticles often tend to form aggregates, and special preparation methods for such materials are used to obtain a more uniform distribution of nanoparticles. The elastic modulus averaging method considered in this paper is also applicable to describe materials with particle aggregates. To do this, it is necessary to first perform the described averaging procedure in each unit separately. It can be expected that the aggregates realize a regime of strong overlap of the effective elastic shells around the individual nanoparticles. The averaging procedure must then be carried out on a larger scale, considering the aggregates as large inclusions with their own elastic moduli.

The results of this study should encourage further study of the elastic properties of amorphous materials both by molecular dynamics methods and experimentally.

6. Conclusion

The macroscopic elastic moduli of amorphous composites are shown to depend on the ratio of the scale of inhomogeneity ξ to some geometric dimension λ. In the case of a thin amorphous layer, there is only the thickness of the layer that determines the size λ. In the case of a composite with spherical particles, the particle radius R, but not the distance between particle centers a, serves as such a size.

At low disorder strength, the macroscopic elastic moduli increase linearly with increasing ratio ξ/λ at the expense of increasing elastic modulus in the near-surface layer with thickness ξ. The macroscopic elastic moduli are proportional to ξ^2/λ^2 in the case of strong disorder, when $\xi \gg \lambda$. In the case of a composite with spherical particles, this quadratic dependence is observed both in case of a weak overlap of the near-surface layers ($R \ll \xi \ll a$) and in case of their strong overlap ($\xi \gg a$).

Acknowledgments

The authors are grateful to D.A. Conyuh for discussion of the results. Y.M. Beltukov is grateful to the Russian Science Foundation for financial support (project № 22-72-10083, https://rscf.ru/en/project/22-72-10083/).

Conflict of interest

The authors declare that they have no conflict of interest.

References

[1] Handbook of Composites, 2nd ed. / S.T. Peters, editor. Springer US, Boston, MA (1998).
[2] T.W. Clyne, D. Hull. An Introduction to Composite Materials, 3rd ed. Cambridge University Press (2019).
[3] Y.W. Mai, Z.Z. Yu. Polymer Nanocomposites. Elsevier Science (2006).
[4] E.T. Thostenson, T.-W. Chou. J. Phys. D: Appl. Phys. **36**, 573 (2003).
[5] M.A. Rafiee, J. Rafiee, Z. Wang, H. Song, Z.-Z. Yu, N. Koratkar. ACS Nano **3**, 3884 (2009).
[6] A. Mesbah, F. Zaïri, S. Boutaleb, J.-M. Gloaguen, M. Naït-Abdelaziz, S. Xie, T. Boukharouba, J.-M. Lefebvre. J. Appl. Polym. Sci. **114**, 3274 (2009).
[7] The Physics of Glassy Polymers / R.N. Haward, R.J. Young, ed. Springer Netherlands, Dordrecht (1997).
[8] T.A. Osswald, G. Menges. Material Science of Polymers for Engineers, 3rd ed. Hanser, Munich (2012).
[9] Polymer Glasses / C.B. Roth, editor. CRC Press, Boca Raton (2017).
[10] S.-Y. Fu, X.-Q. Feng, B. Lauke, Y.-W. Mai. Compos. B: Eng. **39**, 933 (2008).
[11] Y. Ou, F. Yang, Z.-Z. Yu. J. Polym. Sci. B: Polym. Phys. **36**, 789 (1998).
[12] H. Wang, Y. Bai, S. Liu, J. Wu, C.P. Wong. Acta Mater. **50**, 4369 (2002).
[13] B. Wetzel, F. Haupert, M.Q. Zhang. Compos. Sci. Technol. **63**, 2055 (2003).
[14] V.A. Bershtein, O.P. Grigoryeva, P.N. Yakushev, A.M. Fainleib. Polym. Compos. (2021).
[15] D. Stojanovic, A. Orlovic, S. Markovic, V. Radmilovic, P.S. Uskokovic, R. Aleksic. J. Mater. Sci. **44**, 6223 (2009).
[16] P.W. Anderson. Science **267**, 1615 (1995).
[17] C.A. Angell. Proc. Natl. Acad. Sci. **92**, 6675 (1995).
[18] K.L. Ngai. J. Non-Cryst. Solids **353**, 709 (2007).
[19] G.B. McKenna, S.L. Simon. Macromolecules **50**, 6333 (2017).
[20] J. Kang, X. Yang, Q. Hu, Z. Cai, L.-M. Liu, L. Guo. Chem. Rev. **123**, 8859 (2023).
[21] K. Yoshimoto, T.S. Jain, K. Van Workum, P.F. Nealey, J.J. de Pablo. Phys. Rev. Lett. **93**, 175501 (2004).
[22] M. Tsamados, A. Tanguy, C. Goldenberg, J.-L. Barrat. Phys. Rev. E **80**, 026112 (2009).

[23] H. Wagner, D. Bedorf, S. Kuechemann, M. Schwabe, B. Zhang, W. Arnold, K. Samwer. Nat. Mater. **10**, 439 (2011).
[24] H. Mizuno, S. Mossa, J.-L. Barrat. Phys. Rev. E **87**, 042306 (2013).
[25] R. Jana, L. Pastewka. J. Phys. Materials **2**, 045006 (2019).
[26] Q. Wen, A. Basu, P.A. Janmey, A.G. Yodh. Soft Matter. **8**, 8039 (2012).
[27] E. Del Gado, P. Ilg, M. Kröger, H.C. Öttinger. Phys. Rev. Lett. **101**, 095501 (2008).
[28] C. Goldenberg, A. Tanguy, J.-L. Barrat. Europhysics Lett. **80**, 16003 (2007).
[29] F. Leonforte, A. Tanguy, J. Wittmer, J.-L. Barrat. Phys. Rev. Lett. **97**, 055501 (2006).
[30] F. Leonforte, R. Boissière, A. Tanguy, J. Wittmer, J.-L. Barrat. Phys. Rev. B **72**, 224206 (2005).
[31] A. Tanguy, J.P. Wittmer, F. Leonforte, J.-L. Barrat. Phys. Rev. B **66**, 174205 (2002).
[32] G.M. Odegard, T.C. Clancy, T.S. Gates. Polymer **46**, 553 (2005).
[33] F. Bondioli, V. Cannillo, E. Fabbri, M. Messori. J. Appl. Polym. Sci. **97**, 2382 (2005).
[34] S. Saber-Samandari, A. Afaghi-Khatibi. Polym. Compos. **28**, 405 (2007).
[35] R. Qiao, L.C. Brinson. Compos. Sci. Technol. **69**, 491 (2009).
[36] H.W. Wang, H.W. Zhou, R.D. Peng, L. Mishnaevsky Jr. Compos. Sci. Technol. **71**, 980 (2011).
[37] J. Amraei, J.E. Jam, B. Arab, R.D. Firouz-Abadi. J. Compos. Mater. **53**, 1261 (2019).
[38] M. Bazmara, M. Silani, I. Dayyani. Def. Technol. **17**, 177 (2021).
[39] P.F. Brune, G.S. Blackman, T. Diehl, J.S. Meth, D. Brill, Y. Tao, J. Thornton. Macromolecules **49**, 4909 (2016).
[40] N. Ning, T. Mi, G. Chu, L.-Q. Zhang, L. Liu, M. Tian, H.-T. Yu, Y.-L. Lu. Eur. Polym. J. **102**, 10 (2018).
[41] C. Tian, Y. Feng, G. Chu, Y. Lu, C. Miao, N. Ning, L. Zhang, M. Tian. Compos. B Eng. **193**, 108048 (2020).
[42] C. Tian, J. Cui, N. Ning, L. Zhang, M. Tian. Compos. Sci. Technol. **222**, 109367 (2022).
[43] C. Tian, G. Chu, Y. Feng, Y. Lu, C. Miao, N. Ning, L. Zhang, M. Tian. Compos. Sci. Technol. **170**, 1 (2019).
[44] J. Fankhänel, B. Arash, R. Rolfes. Compos. B Eng. **176**, 107211 (2019).
[45] Y.M. Beltukov, D.A. Conyuh, I.A. Solov'yov. Phys. Rev. E **105**, L012501 (2022).
[46] M. Barakat, H. Reda, P. Katsamba, H. Shraim, V. Harmandaris. Mech. Mater. **197**, 105082 (2024).
[47] D. Conyuh, A. Semenov, Y. Beltukov. Phys. Rev. E **108**, 045004 (2023).
[48] Y.M. Beltukov, D.A. Parshin. J. Solid State **53**, 142 (2011).
[49] Y.M. Beltukov, V.I. Kozub, D.A. Parshin. Phys. Rev. B **87**, 134203 (2013).
[50] T. Mori, K. Tanaka. Acta Metall. **21**, 571 (1973).
[51] Y. Benveniste. Mech. Mater. **6**, 147 (1987).
[52] A.A. Semenov, Y.M. Beltukov. Int. J. Solids and Struct. **191**–**192**, 333 (2020).
[53] M.S. Alnæs, J. Blechta, J. Hake, A. Johansson, B. Kehlet, A. Logg, C. Richardson, J. Ring, M.E. Rognes, G.N. Wells. Archive of Numerical Software **3**, 9 (2015).

Translated by A.Akhtyamov